

*SUPPORTING INFORMATION*

Krypton-derivatization highlights O<sub>2</sub>-channeling in a four-electron reducing oxidase

Sylvain Engilberge,<sup>a†</sup> Tristan Wagner,<sup>b†</sup> Philippe Carpentier,<sup>c,d</sup> Eric Girard<sup>e\*</sup> and Seigo Shima<sup>f\*</sup>

[a] Paul Scherrer Institut, Forschungsstrasse 111, 5232 Villigen PSI, Switzerland

[b] Microbial Metabolism Group, Max-Planck-Institut für Marine Mikrobiologie, Celsiusstraße 1,  
28359, Bremen, Germany

[c] Institut de Recherche Interdisciplinaire de Grenoble (IRIG), Laboratoire Chimie et Biologie des  
Métaux (LCBM), Université Grenoble Alpes, CNRS, CEA, Grenoble, France

[d] European Synchrotron Radiation Facility Grenoble, Grenoble, France

[e] Univ. Grenoble Alpes, CEA, CNRS, IBS, F-38000 Grenoble, France

[f] Microbial Protein Structure Group, Max Planck Institute for Terrestrial Microbiology, Karl-von-  
Frisch Straße 10, 35043 Marburg, Germany

† Both authors contributed equally to this work. \*Corresponding authors.

## Methods

### Sample preparation of tFprA in aerobic condition for Kr derivatization

A synthetic DNA of the gene encoding  $F_{420}H_2$  oxidase (FprA) from *Methanothermococcus thermolithotrophicus* was generated, in which the codon usage was optimized for expression in *Escherichia coli* (GeneCust Europe). The gene was synthesized and cloned into the expression plasmid pET-41c (GeneCust Europe). *E. coli* BL21(DE3) cells containing the respective plasmid were grown with shaking at 37 °C overnight in 10 ml Luria-Bertani (LB) medium containing 50 µg/ml kanamycin final. The preculture was inoculated to the 1-l main culture of LB medium supplemented with kanamycin to a final concentration of 50 µg/ml and cultivated with shaking at 37 °C. When the optical density at 600 nm reached 0.6–1.0, the induction was carried out by adding isopropyl-β-D-thiogalactopyranoside to a final concentration of 0.5 mM with shaking for 4 hours at 37 °C. Cells were harvested by centrifugation for 15 min at  $4,500 \times g$ , and the pellet was resuspended in 50 mM Tris-HCl (pH 7.5) containing 20 mM NaCl and 0.1% Triton X-100. After treatment with 0.25 mg/ml lysozyme, 0.05 mg/ml DNaseI, 0.2 mg/ml RNase, cOmplete Protease Inhibitor Cocktail Tablets (Roche) and 10 mM  $MgSO_4$ , the cells were disrupted on ice by sonication by Branson sonifier 150, 3 times for 30 s with intermediary pauses for 30 s. The crude extract was heated at 70 °C for 20 min and then clarified by centrifugation at  $17,000 \times g$  for 45 min at 4 °C. The supernatant was loaded on a 6-ml Resource Q column (GE Healthcare) equilibrated with 20 mM Tris-HCl pH 7.5, 50 mM NaCl. After washing with 3-column volumes (CV) with the equilibration buffer, proteins were eluted at  $3 \text{ ml} \cdot \text{min}^{-1}$  with a 20 CV linear NaCl gradient (0.05 – 0.25 M) in 20 mM Tris-HCl pH 7.5. Fractions corresponding to the elution peak were pooled and

concentrated using an ultrafiltration (Millipore) with a molecular mass cutoff of 50 kDa. The concentrated protein was further purified with Superose 12 column (GE Healthcare).

### **Crystallization, krypton derivatization and structure determination**

Crystals of the FprA protein were obtained by using the HTX-lab crystallization platform EMBL Grenoble. Initial conditions were optimized by the hanging drop method at 293 K using EasyXtalTool X-Seal plates. Large yellow crystals (200 × 50 × 50 μm) were obtained in 100 mM Tris-HCl (pH 8.5) containing 100 mM MgCl<sub>2</sub> and 3.3 to 3.7 M hexanediol. Crystals were harvested using the spoon shape capillaries from MiTeGen. The 'soak-and-freeze' method was then used to perform krypton derivatization during 10 minutes with a pressure of 125 bars before cryo-cooling the crystals still under pressure. The crystals were strickly handled and stored in liquid nitrogen to preserve Kr-FprA complexation stability.<sup>1</sup> Diffraction data were collected on ID29 at the ESRF Grenoble. Two datasets were recorded on the same crystal, below and above the Kr absorption K-edge respectively at 14.2 KeV and 14.4 KeV.

Diffraction frames were integrated using XDS,<sup>2</sup> scaled using CCP4 softwares AIMLESS<sup>3</sup> and POINTLESS.<sup>4</sup> The structure was solved by molecular replacement (Table S2) with PHASER MR<sup>5</sup> using 6FRM as search model. Using the data set collected at 14.4 keV, the position of Krypton atoms was clearly identified in an anomalous Fourier map computed using ANODE (Fig. S7).<sup>6</sup> The model was improved in COOT<sup>7</sup> and refined using BUSTER<sup>8</sup> and PHENIX.<sup>9</sup> For refinement, structure factor of the best dataset (collected at 14.2 KeV) was used. Several iterations of model building and refinement were performed before a final validation using MolProbit<sup>10</sup> and PDB deposition under the PDB id: 6ZLF.

The figures were generated and rendered with PyMOL (version 1.7, Schrödinger). Alignments were performed by Clustal Omega (<http://www.ebi.ac.uk/Tools/msa/clustalo/>). Fig. S1 was made by ESPript 3.0.<sup>11</sup>

### **Anaerobic purification, crystallization and structure determination**

Anaerobic purification and crystallization have been performed as described in Engilberge *et al.* 2019.<sup>12</sup> Anaerobic crystals were grown in a Coy tent containing a gas mixture of H<sub>2</sub>/N<sub>2</sub> at a ratio of 5:95% respectively and were obtained in F2 condition (100 mM TRIS pH 8.5, 40% PEG 400, 200 mM lithium sulfate) from crystallization screen Wizard 3-4, Jena bioscience. A single transparent crystal was harvested and flash frozen in liquid nitrogen. Diffraction data have been collected at SOLEIL synchrotron on PXII beamline. Diffraction frames were integrated using XDS,<sup>2</sup> scaled using CCP4 softwares AIMLESS<sup>3</sup> and POINTLESS.<sup>4</sup> The STARANISO<sup>13</sup> software was used to correct for anisotropy in the diffraction data. The diffraction limits ( $\text{local } (I)/\text{sig}(I) > 1.3$ ) along the h, k, and l axes were 2.35, 1.82, and 1.88 Å, respectively. The structure was solved by molecular replacement (Table S2) with PHASER MR<sup>5</sup> using 6FRM as search model. The model was improved in COOT<sup>7</sup> and refined using BUSTER and PHENIX.<sup>8, 9</sup> Several iterations of model building and refinement were performed before a final validation using MolProbity<sup>10</sup> and PDB deposition under the PDB id: 6ZK8.

### **Structure analysis**

All the figures were realized with PyMoL version 2.4.0. Tunnel detection was performed through the CAVER 3.0.3 plugin in PyMoL. Default parameters, in particular a sphere radius of 0.9 Å, were used and the di-iron centre was used as starting point for channel detection.

SUPPORTING INFORMATION – Figures

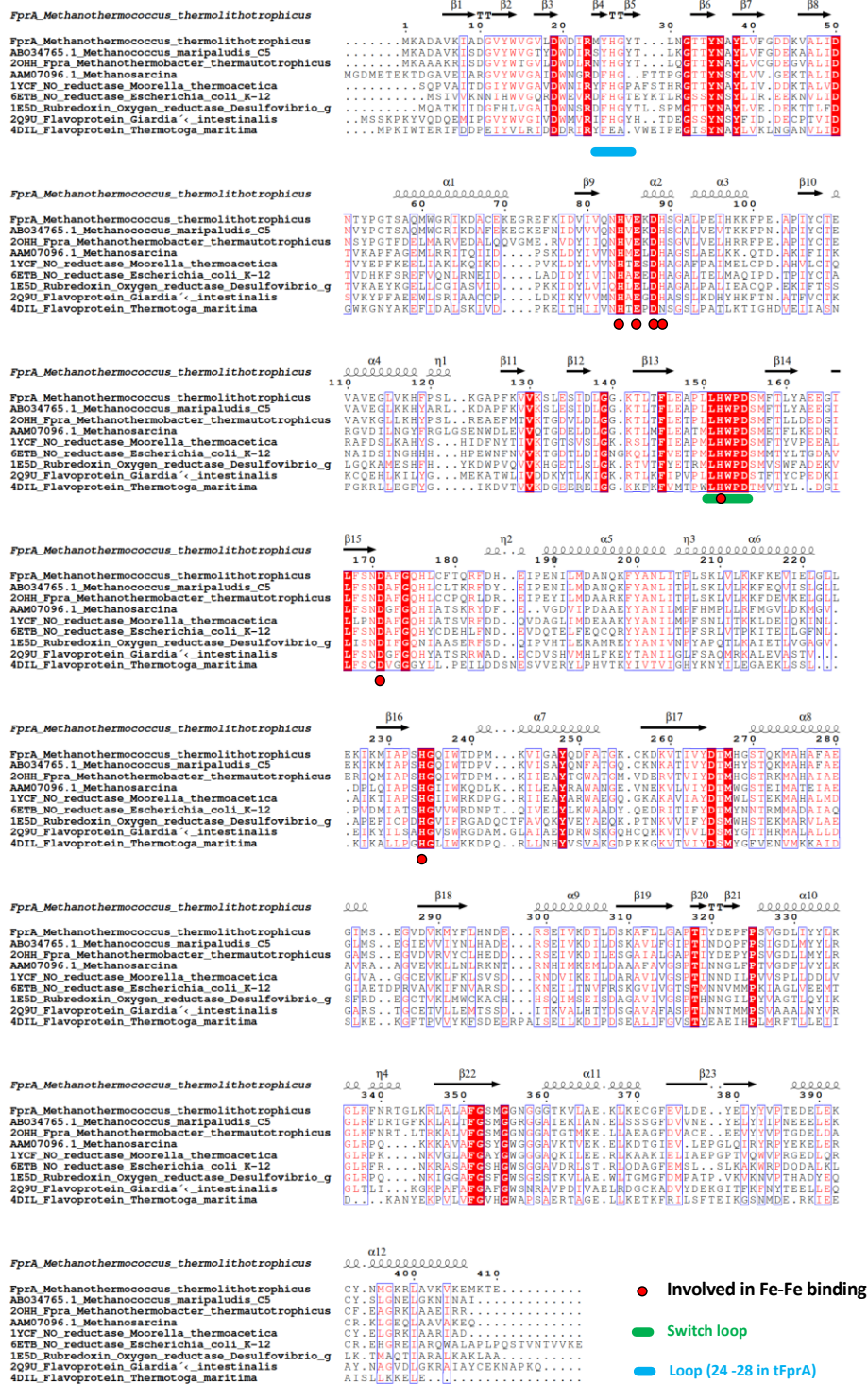
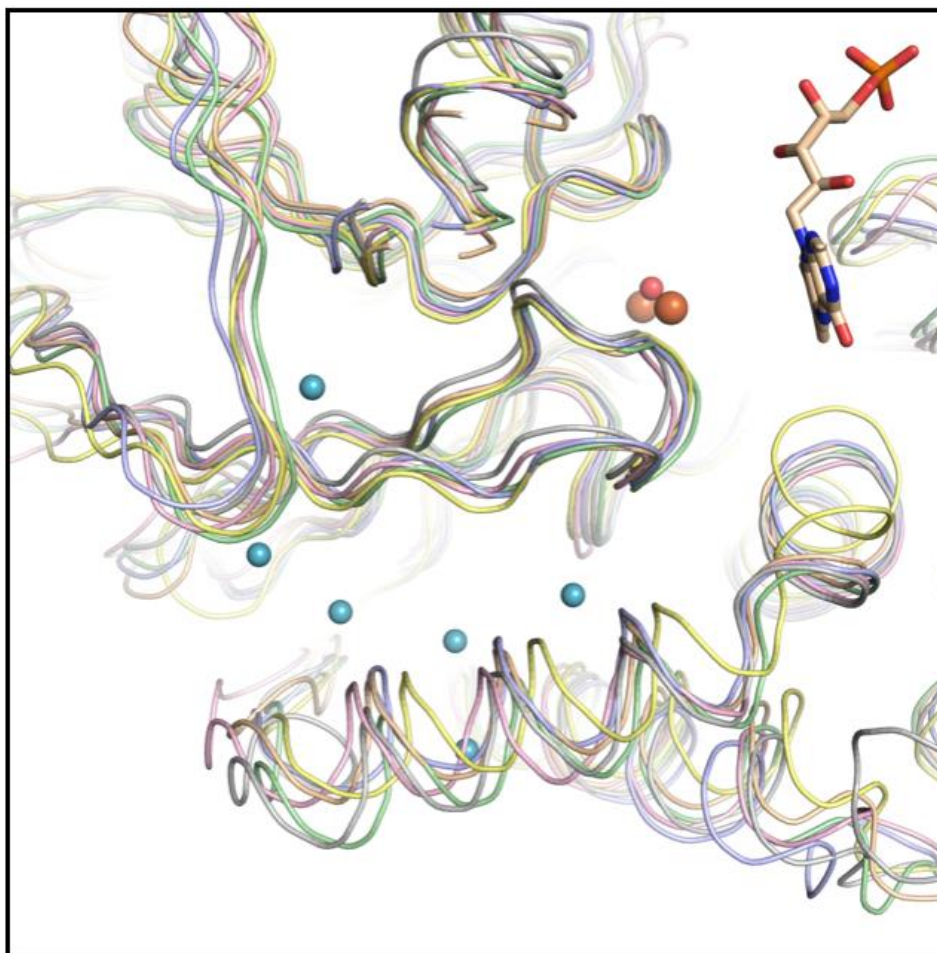
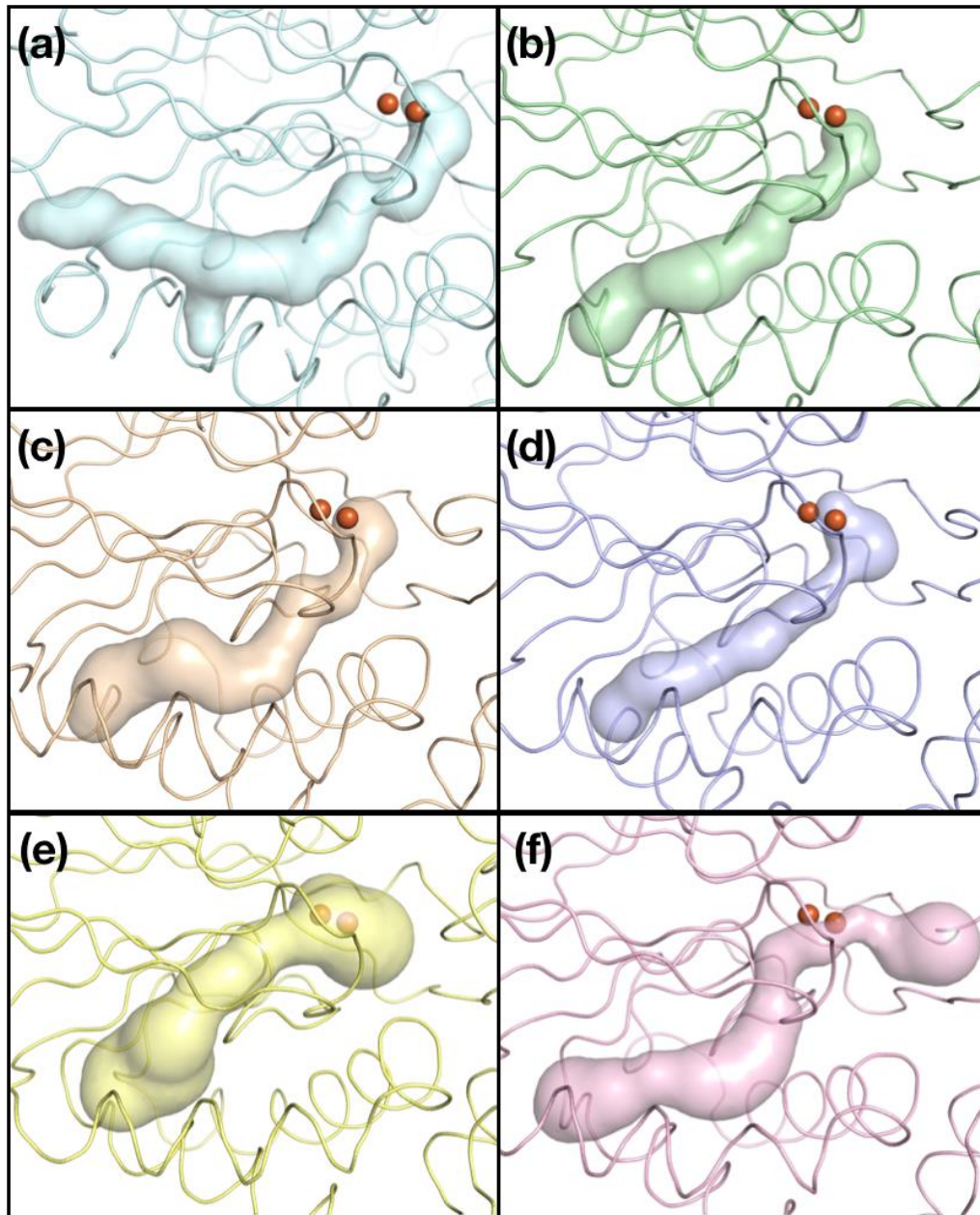


Figure S1. Sequence alignment of FprA homologues with secondary structure elements indicated. The figure was made by ESPript 3.



**Figure S2.** (a) Structure superposition of FprA homologues available in the Protein Data Bank (PDB) showing high fold similarities (C-alpha alignment) around the hydrophobic O<sub>2</sub> channel highlighted by Kr atoms (cyan spheres). FMN (sticks) and di-iron centre (orange spheres) from tFprA<sub>oxo-Kr</sub> structure are also displayed. tFprA<sub>oxo-Kr</sub> in grey, Rubredoxin oxygen reductase from *Desulfovibrio gigas* (PDB: 1E5D) in light orange, NO reductase from *Moorella thermoacetica* (PDB: 1YCF) in green, Flavoprotein from *Giardia intestinalis* (PDB: 2Q9U) in purple, Flavoprotein from *Thermotoga maritima* (PDB: 4DIL) in yellow, NO reductase from *Escherichia coli* K-12 (PDB: 6ETB) in pink.



**Figure S3.** Channels identified by CAVER in FprA homologues available in the Protein Data Bank. Proteins are drawn in ribbon representation, di-iron centre from mFprA (a) is displayed as orange spheres on all the captions. (a) FprA from *Methanothermobacter thermoautotrophicus* (mFprA), reduced state (PDB: 2OHI) in light blue. (b) NO reductase from *Moorella thermoacetica* (PDB: 1YCF) in green. (c) Rubredoxin oxygen reductase from *Desulfovibrio gigas* (PDB: 1E5D) in light orange. (d) Flavoprotein from *Giardia intestinalis* (PDB: 2Q9U) in purple. (e) Flavoprotein from *Thermotoga maritima* (PDB: 4DIL) in yellow. (f) NO reductase from *Escherichia coli* K-12 (PDB: 6ETB) in pink.

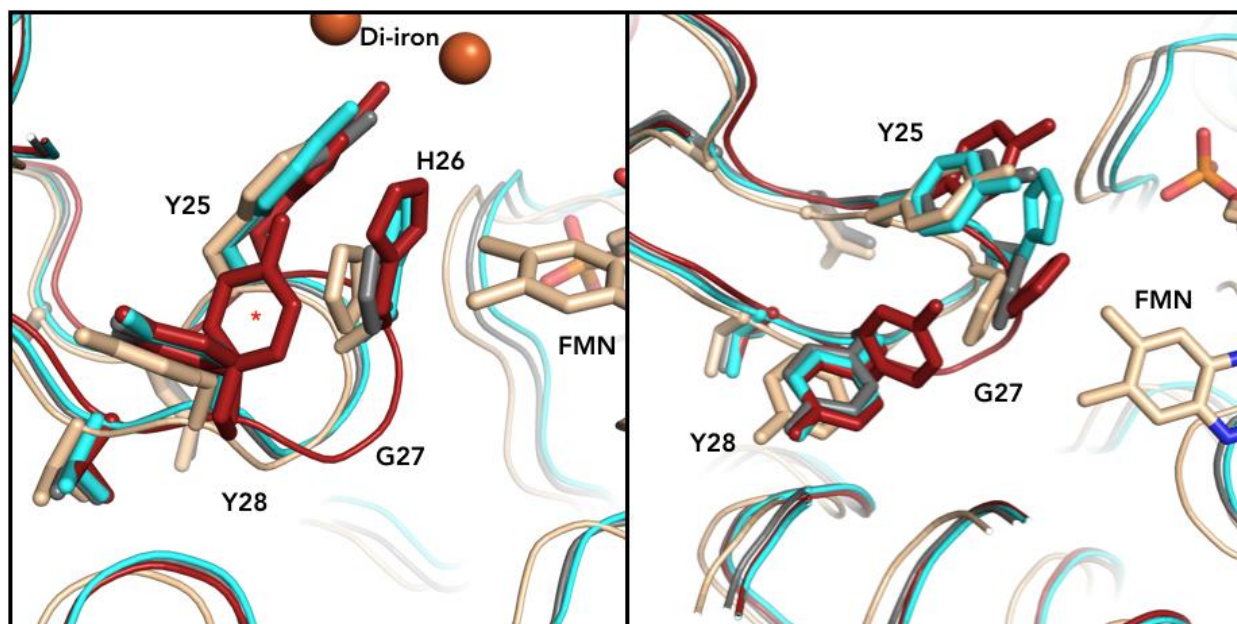


**Figure S4.** Two views of the loop 24-28 in the vicinity of the FMN and catalytic centre. Alignment of mFprA structures 2OHI (grey), 2OHH (orange), tFprA<sub>anox</sub> (red) and tFprA<sub>oxo-Kr</sub> (cyan) display different degree of flexibility. \* (left panel) indicates the main conformation of Y28 tFprA<sub>anox</sub> (occupancy: 70%).

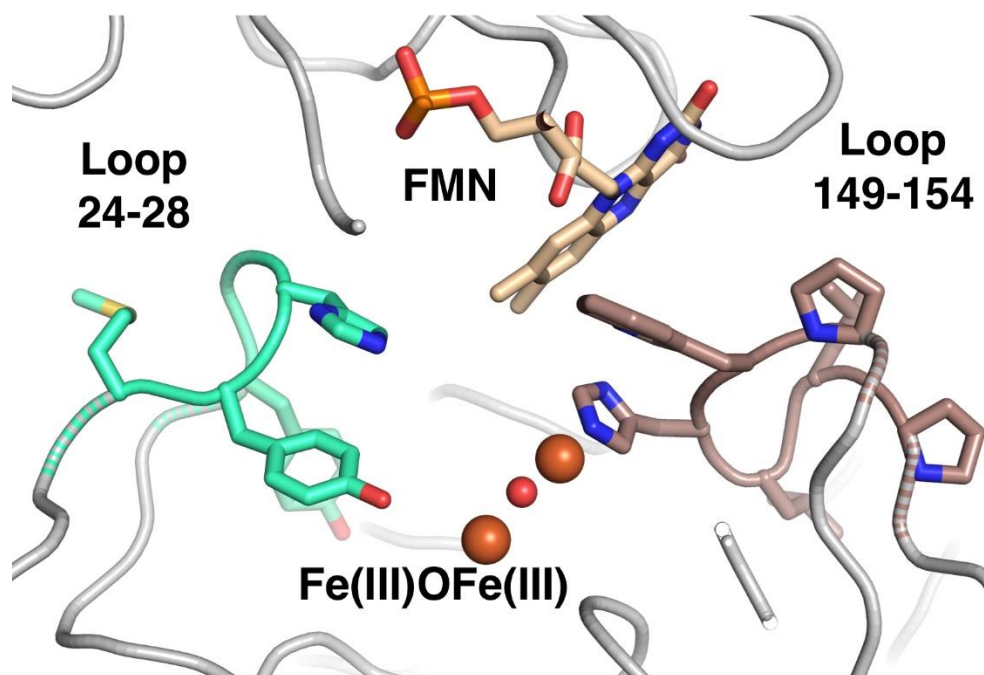


**Figure S5.** The loop 149-154 (brown) coordinating one of the Fe of the di-iron centre (orange spheres) and the loop 24-28 (green) of the tFprA<sub>oxo-Kr</sub> structure. Oxo-bridge (red sphere) and FMN (wheat sticks) are also displayed.

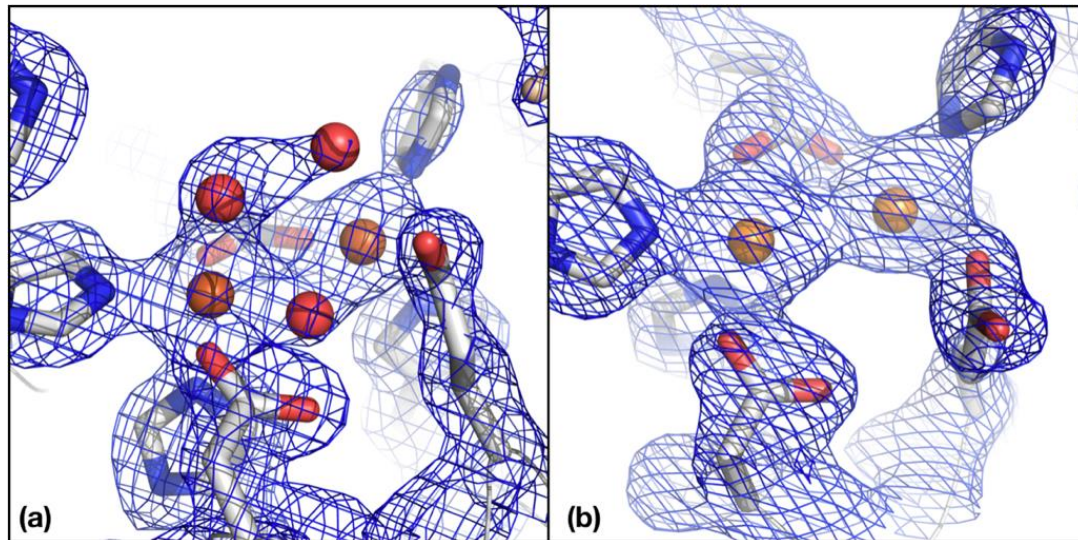


**Figure S6.** (a) tFprA<sub>oxo-Kr</sub> structure showing an oxo-bridge between the two iron atoms (orange) and the presence of putative additional water molecules (red) on the top of the di-iron centre. (b) tFprA<sub>anox</sub> structure showing the two iron atoms (orange) in a reduced state with no water molecule in the close active site environment. Electron densities correspond to  $2F_o-F_c$  maps are contoured at 1 sigma (blue grid).

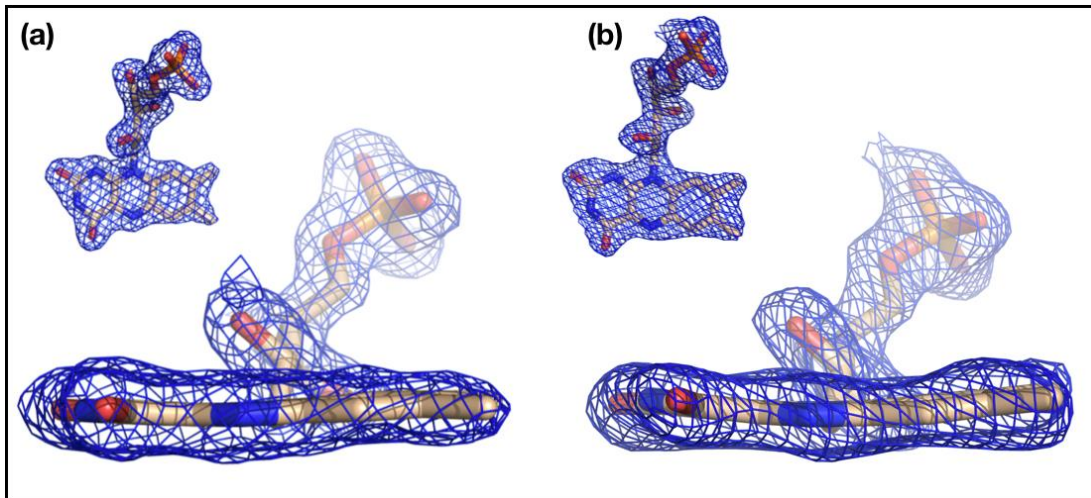


**Figure S7.**  $2F_o-F_c$  map around FMN from (a) tFprA<sub>oxo-Kr</sub> and (b) tFprA<sub>anox</sub> structures. FMN from tFprA<sub>oxo-Kr</sub> and tFprA<sub>anox</sub> seems to be in a partial butterfly conformation. Electron density maps are contoured at 1 sigma (blue grid).

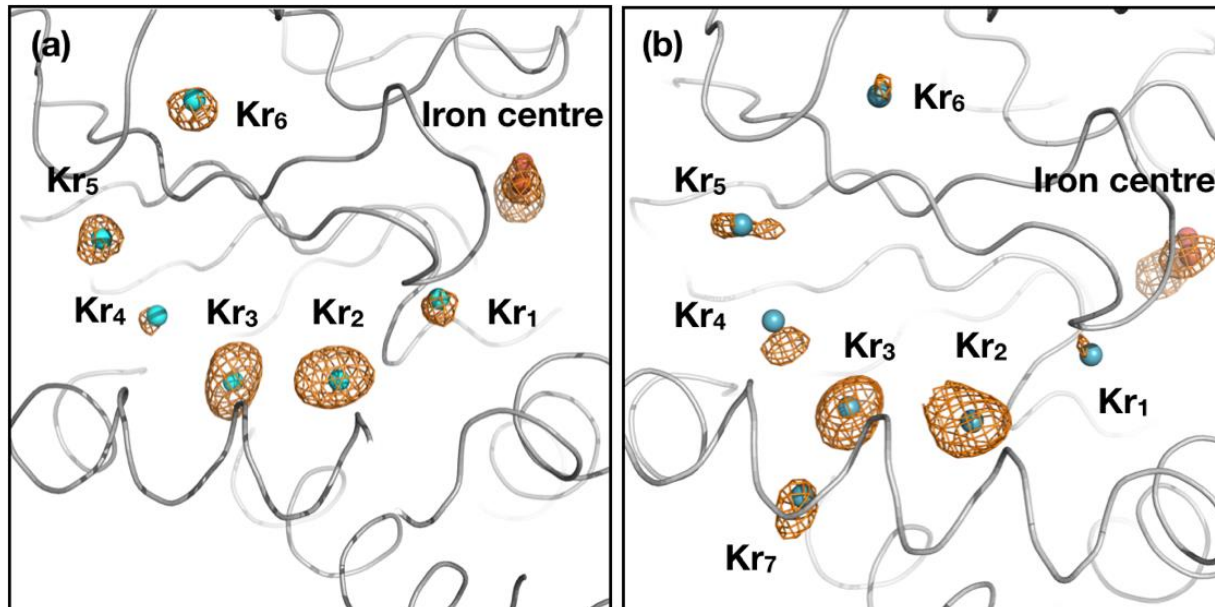


**Figure S8.** Fourier maps (orange grid) computed with ANODE and contoured at 3 sigma around Kr atoms (cyan) in tFprA<sub>oxo-kr</sub> structure. (a) and (b) represent chain I and A respectively. (b) Highlight the presence of an additional Kr binding site (Kr7) found only in two chains (A and H). Di-iron centre is visible on the right part of each captions.

**Table S1.** X-ray data collection, processing and refinement statistics.

<b>Data Collection</b>			
Structure	<b>tFprA<sub>oxo-Kr</sub></b>	<b>tFprA<sub>oxo-Kr</sub></b>	<b>tFprA<sub>anox</sub></b>
Light source	ESRF - ID29	ESRF - ID29	SOLEIL - PXII
Wavelength (KeV)	14.40	14.20	7.52
Space group	<i>P2<sub>1</sub></i>	<i>P2<sub>1</sub></i>	<i>C2<sub>1</sub></i>
Cell constants (Å, °)	75.19 162.72 134.58 90.0, 93.81, 90.0	75.02 162.55 134.37 90.0 93.74 90.0	100.87, 156.61, 76.06 90.0, 137.62, 90.0
Resolution (Å)	49.34 - 1.92 (2.06-1.92)	48.40 - 1.80 (1.86 - 1.80)	43.04 - 1.83 (1.99 - 1.83)
# reflections	1667233 (150108)	2037316 (202707)	145679 (6445)
# unique reflections	241138 (22248)	293871 (29192)	47259 (2363)
Multiplicity	6.90 (6.70)	6.90 (6.90)	3.10 (2.70)
I/σ (I)	8.00 (0.70)	12.84 (1.07)	7.70 (1.30)
Completeness (%)	98.58 (95.10)	99.3 (98.70)	§ 88.8 (48.7)
<i>R</i> <sub>meas</sub> <sup>b</sup> (%)	0.140 (2.563)	0.092 (1.596)	0.094 (0.815)
<i>R</i> <sub>pim</sub> <sup>c</sup> (%)	0.058 (0.965)	0.035 (0.600)	0.051 (0.456)
CC <sub>1/2</sub>	0.999 (0.270)	0.999 (0.465)	0.993 (0.621)
<b>Refinement</b>			
<i>R</i> <sub>work</sub>		17.90	17.81
<i>R</i> <sub>free</sub>		19.12	20.42
rmsd bonds (Å)		0.012	0.009
rmsd angles (°)		1.21	0.86
# molecules in asymmetric unit			
Proteins		8 chains	2 chains
Kr atoms		48	-
Water		2245	535
Ave. B-factor (Å <sup>2</sup> )		38.71	35.44
Clashscore		1.71	1.79
# Ramachandran analysis, % residues in			
favoured regions		97.63	97.43
allowed regions		2.37	2.57
PDB code		6ZLF	6ZK8

<sup>a</sup> Values in parentheses correspond to the highest resolution shell

$$^b R_{\text{meas}} = \frac{\sum_{hkl} \sqrt{(n/n-1) \sum_i |I_i(hkl) - \langle I(hkl) \rangle|}}{\sum_{hkl} \sum_i I_i(hkl)}$$

$$^c R_{\text{pim}} = \frac{\sum_{hkl} \sqrt{(1/n-1) \sum_i |I_i(hkl) - \langle I(hkl) \rangle|}}{\sum_{hkl} \sum_i I_i(hkl)}$$

<sup>d</sup> Calculated in MolProbity

<sup>§</sup> Ellipsoidal completeness after STARANISO

**Table S2.** B-factor analysis of the flexible loop 24-28 involved in the catalytic mechanism.

	<b>tFprA<sub>anox</sub></b> Average B-factor (Å <sup>2</sup> ) at the loop 24-28	<b>tFprA<sub>oxo-kr</sub></b> Average B-factor (Å <sup>2</sup> ) at the loop 24-28	<b>mFprA reduced state (2OHI)</b> Average B-factor (Å <sup>2</sup> ) at the loop 24-28	<b>mFprA oxidized state (2OHH)</b> Average B-factor (Å <sup>2</sup> ) at the loop 24-28
chain A	29.60	60.68	55.87	40.63
chain B	30.50	55.98	56.26	46.71
chain C	-	55.27	56.27	45.37
chain D	-	58.99	55.59	38.19
chain E	-	55.12	55.62	
chain F	-	59.78	56.60	
chain G	-	58.24	55.61	
chain H	-	55.03	56.16	
Loop Av. all chains	<b>30.05</b>	<b>57.39</b>	<b>56.00</b>	<b>42.72</b>
All protein	<b>35.44</b>	<b>38.92</b>	<b>44.11</b>	<b>32.56</b>

## References

1. B. Lafumat, C. Mueller-Dieckmann, G. Leonard, N. Colloc'h, T. Prange, T. Giraud, F. Dobias, A. Royant, P. van der Linden and P. Carpentier, *J. Appl. Cryst.*, 2016, **49**, 1478-1487.
2. W. Kabsch, *Acta Crystallogr., Sect. D*, 2010, **66**, 125-132.
3. P. R. Evans and G. N. Murshudov, *Acta Crystallogr., Sect. D*, 2013, **69**, 1204-1214.
4. P. R. Evans, *Acta Crystallogr., Sect. D*, 2011, **67**, 282-292.
5. A. J. McCoy, R. W. Grosse-Kunstleve, P. D. Adams, M. D. Winn, L. C. Storoni and R. J. Read, *J. Appl. Crystallogr.*, 2007, **40**, 658-674.
6. A. Thorn and G. M. Sheldrick, *J. Appl. Crystallogr.*, 2011, **44**, 1285-1287.
7. P. Emsley and K. Cowtan, *Acta Crystallogr., Sect. D*, 2004, **60**, 2126-2132.
8. G. Bricogne, E. Blanc, M. Brandl, C. Flensburg, P. Keller, W. Paciorek, P. Roversi, A. Sharff, O. Smart, C. Vonrhein and T. O. Womack, *Cambridge, United Kingdom: Global Phasing Ltd.*, 2016.
9. P. V. Afonine, R. W. Grosse-Kunstleve, V. B. Chen, J. J. Headd, N. W. Moriarty, J. S. Richardson, D. C. Richardson, A. Urzhumtsev, P. H. Zwart and P. D. Adams, *J. Appl. Crystallogr.*, 2010, **43**, 669-676.
10. V. B. Chen, W. B. Arendall III, J. J. Headd, D. A. Keedy, R. M. Immormino, G. J. Kapral, L. W. Murray, J. S. Richardson and D. C. Richardson, *Acta Crystallogr. D*, 2010, **66**, 12-21.
11. X. Robert and P. Gouet, *Nucleic Acids Res.*, 2014, **42**, W320-W324.
12. S. Engilberge, T. Wagner, G. Santoni, C. Breyton, S. Shima, B. Franzetti, F. Riobé, O. Maury and E. Girard, *J. Appl. Crystallogr.*, 2019, **52**, 722-731.
13. I. J. Tickle, C. Flensburg, P. Keller, W. Paciorek, A. Sharff, C. Vonrhein and G. Bricogne, *Cambridge, United Kingdom: Global Phasing Ltd.*, 2018.